

Generalized Multiscale Finite Element Method for Elasticity Equations

Eric T. Chung*, Yalchin Efendiev[†] and Shubin Fu[‡]

September 17, 2018

Abstract

In this paper, we discuss the application of Generalized Multiscale Finite Element Method (GMsFEM) to elasticity equation in heterogeneous media. Our applications are motivated by elastic wave propagation in subsurface where the subsurface properties can be highly heterogeneous and have high contrast. We present the construction of main ingredients for GMsFEM such as the snapshot space and offline spaces. The latter is constructed using local spectral decomposition in the snapshot space. The spectral decomposition is based on the analysis which is provided in the paper. We consider both continuous Galerkin and discontinuous Galerkin coupling of basis functions. Both approaches have their cons and pros. Continuous Galerkin methods allow avoiding penalty parameters though they involve partition of unity functions which can alter the properties of multiscale basis functions. On the other hand, discontinuous Galerkin techniques allow gluing multiscale basis functions without any modifications. Because basis functions are constructed independently from each other, this approach provides an advantage. We discuss the use of oversampling techniques that use snapshots in larger regions to construct the offline space. We provide numerical results to show that one can accurately approximate the solution using reduced number of degrees of freedom.

1 Introduction

Many materials in nature are highly heterogeneous and their properties can vary at different scales. Direct numerical simulations in such multiscale media are prohibitively expensive and some type of model reduction is needed. Multiscale approaches such as homogenization and numerical homogenization [3, 1, 14, 2, 10, 13, 15, 12] have been routinely used to model macroscopic properties and macroscopic behavior of elastic materials. These approaches compute the effective material properties based on representative volume simulations. These properties are further used to solve macroscale equations. In this paper, our goal is to design multiscale method for elasticity equations in the media when the media properties do not have scale separation and classical homogenization and numerical homogenization techniques do not work. We are motivated by seismic wave applications when elastic wave propagation in heterogeneous subsurface formation is studied where the subsurface properties can contain vugs, fractures, and cavities of different sizes. In this paper, we develop multiscale methods for static problems and present their analysis.

In this paper, we design a multiscale model reduction techniques using GMsFEM for steady state elasticity equation in heterogeneous media

$$\frac{\partial}{\partial x_i}(c_{ijkl}(x)e_{kl}(u)) = f_j(x), \quad (1)$$

*Department of Mathematics, The Chinese University of Hong Kong, Hong Kong SAR. This research is partially supported by the Hong Kong RGC General Research Fund (Project number: 400411).

[†]Department of Mathematics, Texas A&M University, College Station, TX 77843 and Numerical Porous Media SRI Center, KAUST, Thuwal, Saudia Arabia

[‡]Department of Mathematics, Texas A&M University, College Station, TX 77843.

where $e_{kl}(u) = \frac{1}{2}(\frac{\partial u_k}{\partial x_l} + \frac{\partial u_l}{\partial x_k})$ and $c_{ijkl}(x)$ is a multiscale field with a high contrast. GMsFEM has been studied for a various applications related to flow problems (see [5, 7, 4, 9, 8]). In GMsFEM, we solve equation (1) on a coarse grid where each coarse grid consists of a union of fine-grid blocks. In particular, we design (1) a snapshot space (2) an offline space for each coarse patch. The offline space consists of multiscale basis functions that are coupled in a global formulation. In this paper, we consider several choices for snapshot spaces, offline spaces, and global coupling. The main idea of the snapshot space in each coarse patch is to provide an exhaustive space where an appropriate spectral decomposition is performed. This space contains local functions that can mimic the global solution behavior in the coarse patch for all right hand sides or boundary conditions. We consider two choices for the snapshot space. The first one consists of all fine-grid functions in each coarse patch and the second one consists of harmonic extensions. Next, we propose a local spectral decomposition in the snapshot space which allows selecting multiscale basis functions. This local spectral decomposition is based on the analysis and depends on the global coupling mechanisms. We consider several choices for the local spectral decomposition including oversampling approach where larger domains are used in the eigenvalue problem. The oversampling technique uses larger domains to compute snapshot vectors that are more consistent with local solution space and thus can have much lower dimension.

To couple multiscale basis functions constructed in the offline space, we consider two methods, conforming Galerkin (CG) approach and discontinuous Galerkin (DG) approach based on symmetric interior penalty method for (1). These approaches are studied for linear elliptic equations in [5, 6]. Both approaches provide a global coupling for multiscale basis functions where the solution is sought in the space spanned by these multiscale basis functions. This representation allows approximating the solution with a reduced number of degrees of freedom. The constructions of the basis functions are different for continuous Galerkin and discontinuous Galerkin methods as the local spectral decomposition relies on the analysis. In particular, for continuous Galerkin approach, we use partition of unity functions and discuss several choices for partition of unity functions. We provide an analysis of both approaches. The offline space construction is based on the analysis.

We present numerical results where we study the convergence of continuous and discontinuous Galerkin methods using various snapshot spaces as well as with and without the use of oversampling. We consider highly heterogeneous coefficients that contain high contrast. Our numerical results show that the proposed approaches allow approximating the solution accurately with a fewer degrees of freedom. In particular, when using the snapshot space consisting of harmonic extension functions, we obtain better convergence results. In addition, oversampling methods and the use of snapshot spaces constructed in the oversampled domains can substantially improve the convergence.

The paper is organized as follows. In Section 2, we state the problem and the notations for coarse and fine grids. In Section 3, we give the construction of multiscale basis functions, snapshot spaces and offline spaces, as well as global coupling via CG and DG. In Section 4, we present numerical results. Sections 5-6 are devoted to the analysis of the methods.

2 Preliminaries

In this section, we will present the general framework of GMsFEM for linear elasticity in high-contrast media. Let $D \subset \mathbb{R}^2$ (or \mathbb{R}^3) be a bounded domain representing the elastic body of interest, and let $u = (u_1, u_2)$ be the displacement field. The strain tensor $\epsilon(u) = (\epsilon_{ij}(u))_{1 \leq i, j \leq 2}$ is defined by

$$\epsilon(u) = \frac{1}{2}(\nabla u + \nabla u^T),$$

where $\nabla u = (\frac{\partial u_i}{\partial x_j})_{1 \leq i, j \leq 2}$. In the component form, we have

$$\epsilon_{ij}(u) = \frac{1}{2}\left(\frac{\partial u_i}{\partial x_j} + \frac{\partial u_j}{\partial x_i}\right), \quad 1 \leq i, j \leq 2.$$

In this paper, we assume the medium is isotropic. Thus, the stress tensor $\sigma(u) = (\sigma_{ij}(u))_{1 \leq i, j \leq 2}$ is related to the strain tensor $\epsilon(u)$ in the following way

$$\sigma = 2\mu\epsilon + \lambda\nabla \cdot u I,$$

where $\lambda > 0$ and $\mu > 0$ are the Lamé coefficients. We assume that λ and μ have highly heterogeneous spatial variations with high contrasts. Given a forcing term $f = (f_1, f_2)$, the displacement field u satisfies the following

$$-\nabla \cdot \sigma = f, \quad \text{in } D \quad (2)$$

or in component form

$$-\left(\frac{\partial \sigma_{i1}}{\partial x_1} + \frac{\partial \sigma_{i2}}{\partial x_2}\right) = f_i, \quad \text{in } D, \quad i = 1, 2. \quad (3)$$

For simplicity, we will consider the homogeneous Dirichlet boundary condition $u = 0$ on ∂D .

Let \mathcal{T}^H be a standard triangulation of the domain D where $H > 0$ is the mesh size. We call \mathcal{T}^H the coarse grid and H the coarse mesh size. Elements of \mathcal{T}^H are called coarse grid blocks. The set of all coarse grid edges is denoted by \mathcal{E}^H and the set of all coarse grid nodes is denoted by \mathcal{S}^H . We also use N_S to denote the number of coarse grid nodes, N to denote the number of coarse grid blocks. In addition, we let \mathcal{T}^h be a conforming refinement of the triangulation \mathcal{T}^H . We call \mathcal{T}^h the fine grid and $h > 0$ is the fine mesh size. We remark that the use of the conforming refinement is only to simplify the discussion of the methodology and is not a restriction of the method.

Let V^h be a finite element space defined on the fine grid. The fine-grid solution u_h can be obtained as

$$a(u_h, v) = (f, v), \quad \forall v \in V^h, \quad (4)$$

where

$$a(u, v) = \int_D \left(2\mu\epsilon(u) : \epsilon(v) + \lambda\nabla \cdot u \nabla \cdot v\right) dx, \quad (f, v) = \int_D f \cdot v dx \quad (5)$$

and

$$\epsilon(u) : \epsilon(v) = \sum_{i,j=1}^2 \epsilon_{ij}(u)\epsilon_{ij}(v), \quad f \cdot v = \sum_{i=1}^2 f_i v_i. \quad (6)$$

Now, we present GMsFEM. The discussion consists of two main steps, namely, the construction of local basis functions and the global coupling. In this paper, we will develop and analyze two types of global coupling, namely, the continuous Galerkin coupling and the discontinuous Galerkin coupling. These two couplings will require two types of local basis functions. In essence, the CG coupling will need vertex-based local basis functions and the DG coupling will need element-based local basis functions.

For each vertex $x_i \in \mathcal{S}^H$ in the coarse grid, we define the coarse neighborhood ω_i by

$$\omega_i = \bigcup \{K_j : K_j \subset \mathcal{T}^H, x_i \in K_j\}.$$

That is, ω_i is the union of all coarse grid blocks K_j having the vertex x_i (see Figure 1). A snapshot space $V^{i,\text{snap}}$ is constructed for each coarse neighborhood ω_i . The snapshot space contains a large set that represents the local solution space. A spectral problem is then constructed to get a reduced dimensional space. Specifically, the spectral problem is solved in the snapshot space and eigenfunctions corresponding to dominant modes are used as the final basis functions. To obtain conforming basis functions, each of these selected modes will be multiplied by a partition of unity function. The resulting space is denoted by $V^{i,\text{off}}$, which is called the offline space for the i -th coarse neighborhood ω_i . The global offline space V^{off} is then defined as the linear span of all these $V^{i,\text{off}}$, for $i = 1, 2, \dots, N_S$. The CG coupling can be formulated as to find $u_H^{\text{CG}} \in V^{\text{off}}$ such that

$$a(u_H^{\text{CG}}, v) = (f, v), \quad \forall v \in V^{\text{off}}. \quad (7)$$

The DG coupling can be constructed in a similar fashion. A snapshot space $V^{i,\text{snap}}$ is constructed for each coarse grid block K_i . A spectral problem is then solved in the snapshot space and eigenfunctions

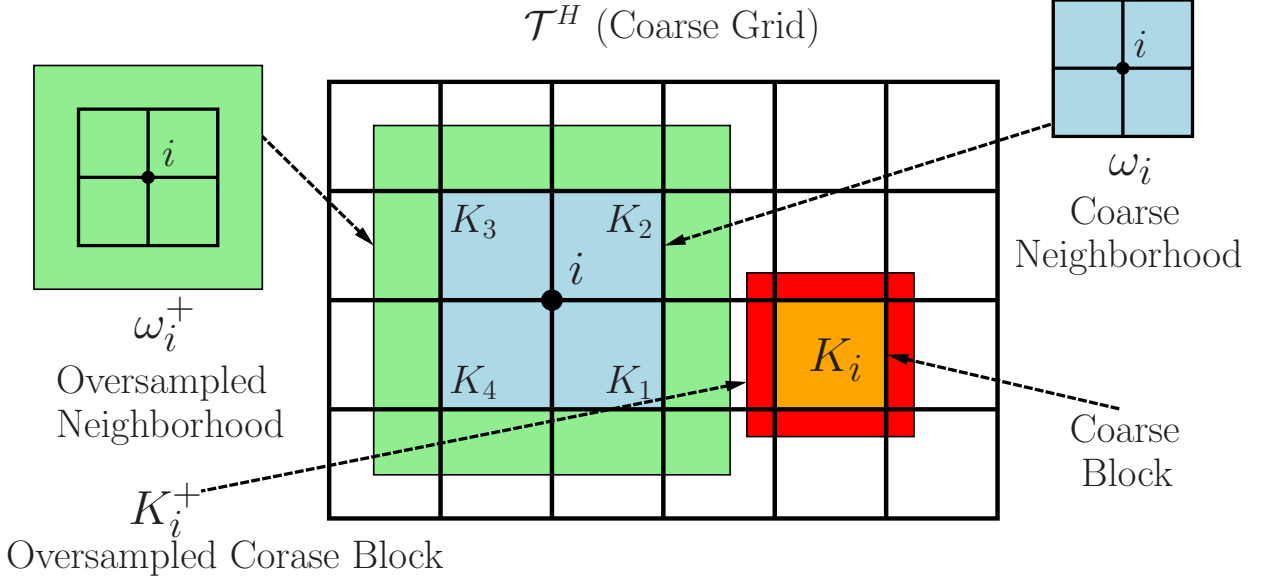


Figure 1: Illustration of a coarse neighborhood, oversampled coarse neighborhood, coarse block and oversampled coarse block.

corresponding to dominant modes are used as the final basis functions. This space is called the offline space $V^{i,\text{off}}$ for the i -th coarse grid block. The global offline space V^{off} is then defined as the linear span of all these $V^{i,\text{off}}$, for $i = 1, 2, \dots, N$. The DG coupling can be formulated as: find $u_H^{\text{DG}} \in V^{\text{off}}$ such that

$$a_{\text{DG}}(u_H^{\text{DG}}, v) = (f, v), \quad \forall v \in V^{\text{off}}, \quad (8)$$

where the bilinear form a_{DG} is defined as

$$a_{\text{DG}}(u, v) = a_H(u, v) - \sum_{E \in \mathcal{E}^H} \int_E \left(\{\sigma(u) n_E\} \cdot [v] + \{\sigma(v) n_E\} \cdot [u] \right) ds + \sum_{E \in \mathcal{E}^H} \frac{\gamma}{h} \int_E \{\lambda + 2\mu\} [u] \cdot [v] ds \quad (9)$$

with

$$a_H(u, v) = \sum_{K \in \mathcal{T}_H} a_H^K(u, v), \quad a_H^K(u, v) = \int_K \left(2\mu \epsilon(u) : \epsilon(v) + \lambda \nabla \cdot u \nabla \cdot v \right) dx, \quad (10)$$

where $\gamma > 0$ is a penalty parameter, n_E is a fixed unit normal vector defined on the coarse edge E and $\sigma(u) n_E$ is a matrix-vector product. Note that, in (9), the average and the jump operators are defined in the classical way. Specifically, consider an interior coarse edge $E \in \mathcal{E}^H$ and let K^+ and K^- be the two coarse grid blocks sharing the edge E . For a piecewise smooth function G , we define

$$\{G\} = \frac{1}{2}(G^+ + G^-), \quad \llbracket G \rrbracket = G^+ - G^-, \quad \text{on } E,$$

where $G^+ = G|_{K^+}$ and $G^- = G|_{K^-}$ and we assume that the normal vector n_E is pointing from K^+ to K^- . For a coarse edge E lying on the boundary ∂D , we define

$$\{G\} = \llbracket G \rrbracket = G, \quad \text{on } E,$$

where we always assume that n_E is pointing outside of D . For vector-valued functions, the above average and jump operators are defined component-wise. We note that the DG coupling (8) is the classical interior penalty discontinuous Galerkin (IPDG) method with our multiscale basis functions.

Finally, we remark that, we use the same notations $V^{i,\text{snap}}$, $V^{i,\text{off}}$ and V^{off} to denote the local snapshot, local offline and global offline spaces for both the CG coupling and the DG coupling to simplify notations.

3 Construction of multiscale basis functions

This section is devoted to the construction of multiscale basis functions.

3.1 Basis functions for CG coupling

We begin by the construction of local snapshot spaces. Let ω_i be a coarse neighborhood, $i = 1, 2, \dots, N_S$. We will define two types of local snapshot spaces. The first type of local snapshot space is

$$V_1^{i,\text{snap}} = V^h(\omega_i),$$

where $V^h(\omega_i)$ is the restriction of the conforming space to ω_i . Therefore, $V_1^{i,\text{snap}}$ contains all possible fine scale functions defined on ω_i . The second type of local snapshot space contains all possible harmonic extensions. Next, let $V^h(\partial\omega_i)$ be the restriction of the conforming space to $\partial\omega_i$. Then we define the fine-grid delta function $\delta_k \in V^h(\partial\omega_i)$ on $\partial\omega_i$ by

$$\delta_k(x_l) = \begin{cases} 1, & l = k \\ 0, & l \neq k, \end{cases}$$

where $\{x_l\}$ are all fine grid nodes on $\partial\omega_i$. Given δ_k , we find u_{k1} and u_{k2} by

$$\begin{aligned} -\nabla \cdot \sigma(u_{k1}) &= 0, & \text{in } \omega_i \\ u_{k1} &= (\delta_k, 0)^T, & \text{on } \partial\omega_i \end{aligned} \tag{11}$$

and

$$\begin{aligned} -\nabla \cdot \sigma(u_{k2}) &= 0, & \text{in } \omega_i \\ u_{k2} &= (0, \delta_k)^T, & \text{on } \partial\omega_i. \end{aligned} \tag{12}$$

The linear span of the above harmonic extensions is our second type of local snapshot space $V_2^{i,\text{snap}}$. To simplify the notations, we will use $V^{i,\text{snap}}$ to denote $V_1^{i,\text{snap}}$ or $V_2^{i,\text{snap}}$ when there is no need to distinguish the two type of spaces. Moreover, we write

$$V^{i,\text{snap}} = \text{span}\{\psi_k^{i,\text{snap}}, \quad k = 1, 2, \dots, M^{i,\text{snap}}\},$$

where $M^{i,\text{snap}}$ is the number of basis functions in $V^{i,\text{snap}}$.

We will perform a dimension reduction on the above snapshot spaces by the use of a spectral problem. First, we will need a partition of unity function χ_i for the coarse neighborhood ω_i . One choice of a partition of unity function is the coarse grid hat functions Φ_i , that is, the piecewise bi-linear function on the coarse grid having value 1 at the coarse vertex x_i and value 0 at all other coarse vertices. The other choice is the multiscale partition of unity function, which is defined in the following way. Let K_j be a coarse grid block having the vertex x_i . Then we consider

$$\begin{aligned} -\nabla \cdot \sigma(\zeta_i) &= 0, & \text{in } K_j \\ \zeta_i &= (\Phi_i, 0)^T, & \text{on } \partial K_j. \end{aligned} \tag{13}$$

Then we define the multiscale partition of unity as $\tilde{\Phi}_i = (\zeta_i)_1$. The values of $\tilde{\Phi}_i$ on the other coarse grid blocks are defined similarly.

Based on our analysis to be presented in the next sections, we define the spectral problem as

$$\int_{\omega_i} \left(2\mu\epsilon(u) : \epsilon(v) + \lambda \nabla \cdot u \nabla \cdot v \right) dx = \xi \int_{\omega_i} \tilde{\kappa} u \cdot v dx, \tag{14}$$

where ξ denotes the eigenvalue and

$$\tilde{\kappa} = \sum_{i=1}^{N_S} (\lambda + 2\mu) |\nabla \chi_i|^2. \quad (15)$$

The above spectral problem (14) is solved in the snapshot space. We let (ϕ_k, ξ_k) be the eigenfunctions and the corresponding eigenvalues. Assume that

$$\xi_1 \leq \xi_2 \leq \dots \leq \xi_{M^{i,\text{snap}}}.$$

Then the first L_i eigenfunctions will be used to construct the local offline space. We define

$$\psi_l^{i,\text{off}} = \sum_{k=1}^{M^{i,\text{snap}}} \phi_{lk} \psi_k^{i,\text{snap}}, \quad l = 1, 2, \dots, L_i, \quad (16)$$

where ϕ_{lk} is the k -th component of ϕ_l . The local offline space is then defined as

$$V^{i,\text{off}} = \text{span}\{\chi_i \psi_l^{i,\text{off}}, \quad l = 1, 2, \dots, L_i\}.$$

Next, we define the global continuous Galerkin offline space as

$$V^{\text{off}} = \text{span}\{V^{i,\text{off}}, \quad i = 1, 2, \dots, N_S\}.$$

3.2 Basis functions for DG coupling

We will construct the local basis functions required for the DG coupling. We also provide two types of snapshot spaces as in CG case. The first type of local snapshot space is all possible fine grid bi-linear functions defined on K_i . The second type of local snapshot space $V^{i,\text{snap}}$ for the coarse grid block K_i is defined as the linear span of all harmonic extensions. Specifically, given δ_k , we find u_{k1} and u_{k2} by

$$\begin{aligned} -\nabla \cdot \sigma(u_{k1}) &= 0, & \text{in } K_i \\ u_{k1} &= (\delta_k, 0)^T, & \text{on } \partial K_i \end{aligned} \quad (17)$$

and

$$\begin{aligned} -\nabla \cdot \sigma(u_{k2}) &= 0, & \text{in } K_i \\ u_{k2} &= (0, \delta_k)^T, & \text{on } \partial K_i. \end{aligned} \quad (18)$$

The linear span of the above harmonic extensions is the local snapshot space $V^{i,\text{snap}}$. We also write

$$V^{i,\text{snap}} = \text{span}\{\psi_k^{i,\text{snap}}, \quad k = 1, 2, \dots, M^{i,\text{snap}}\},$$

where $M^{i,\text{snap}}$ is the number of basis functions in $V^{i,\text{snap}}$.

We will perform a dimension reduction on the above snapshot spaces by the use of a spectral problem. Based on our analysis to be presented in the next sections, we define the spectral problem as

$$\int_{K_i} (2\mu \epsilon(u) : \epsilon(v) + \lambda \nabla \cdot u \nabla \cdot v) dx = \frac{\xi}{H} \int_{\partial K_i} \langle \lambda + 2\mu \rangle u \cdot v ds, \quad (19)$$

where ξ denotes the eigenvalues and $\langle \lambda + 2\mu \rangle$ is the maximum value of $\{\lambda + 2\mu\}$ on ∂K_i . The above spectral problem (19) is again solved in the snapshot space $V^{i,\text{snap}}$. We let (ϕ_k, ξ_k) , for $k = 1, 2, \dots, M^{i,\text{snap}}$ be the eigenfunctions and the corresponding eigenvalues. Assume that

$$\xi_1 \leq \xi_2 \leq \dots \leq \xi_{M^{i,\text{snap}}}.$$

Then the first L_i eigenfunctions will be used to construct the local offline space. Indeed, we define

$$\psi_l^{i,\text{off}} = \sum_{k=1}^{M^{i,\text{snap}}} \phi_{lk} \psi_k^{i,\text{snap}}, \quad l = 1, 2, \dots, L_i, \quad (20)$$

where ϕ_{lk} is the k -th component of ϕ_l . The local offline space is then defined as

$$V^{i,\text{off}} = \text{span}\{\psi_l^{i,\text{off}}, \quad l = 1, 2, \dots, L_i\}.$$

The global offline space is also defined as

$$V^{\text{off}} = \text{span}\{V^{i,\text{off}}, \quad i = 1, 2, \dots, N\}.$$

3.3 Oversampling technique

In this section, we present an oversampling technique for generating multiscale basis functions. The main idea of oversampling is to solve local spectral problem in a larger domain. This allows obtaining a snapshot space that has a smaller dimension since snapshot vectors contain solution oscillation near the boundaries. In our previous approaches, we assume that the snapshot vectors can have an arbitrary value on the boundary of coarse blocks which yield to large dimensional coarse spaces.

For the harmonic extension snapshot case, we solve equation (11) and (12) in ω_i^+ (see Figure 1) instead of ω_i for CG case, and solve the equation (17) and (18) in K_i^+ instead of K_i for DG case. We denote the solutions as $\psi_i^{+,\text{snap}}$, and their restrictions on ω_i or K_i as ψ_i^{snap} . We reorder these functions according eigenvalue behavior and write

$$R_{\text{snap}}^+ = [\psi_1^{+,\text{snap}}, \dots, \psi_{M_{\text{snap}}}^{+,\text{snap}}] \quad \text{and} \quad R_{\text{snap}} = [\psi_1^{\text{snap}}, \dots, \psi_{M_{\text{snap}}}^{\text{snap}}].$$

where M_{snap} denotes the total number of functions kept in the snapshot space.

For CG case we define the following spectral problems in the space of snapshot:

$$R_{\text{snap}}^T A R_{\text{snap}} \Psi_k = \zeta (R_{\text{snap}}^+)^T M^+ R_{\text{snap}}^+ \Psi_k, \quad (21)$$

or

$$(R_{\text{snap}}^+)^T A^+ R_{\text{snap}}^+ \Psi_k = \zeta (R_{\text{snap}}^+)^T M^+ R_{\text{snap}}^+ \Psi_k, \quad (22)$$

where

$$\begin{aligned} A &= [a_{kl}] = \int_{\omega_i} \left(2\mu \epsilon(\psi_k^{\text{snap}}) : \epsilon(\psi_l^{\text{snap}}) + \lambda \nabla \cdot \psi_k^{\text{snap}} \nabla \cdot \psi_l^{\text{snap}} \right) dx, \\ A^+ &= [a_{kl}^+] = \int_{\omega_i^+} \left(2\mu \epsilon(\psi_k^{+,\text{snap}}) : \epsilon(\psi_l^{+,\text{snap}}) + \lambda \nabla \cdot \psi_k^{+,\text{snap}} \nabla \cdot \psi_l^{+,\text{snap}} \right) dx, \\ M^+ &= [m_{kl}^+] = \int_{\omega_i^+} \tilde{\kappa} \psi_k^{+,\text{snap}} \cdot \psi_l^{+,\text{snap}} dx, \end{aligned}$$

where $\tilde{\kappa}$ is defined through (15).

The local spectral problem for DG coupling is defined as

$$(R_{\text{snap}}^+)^T A^+ R_{\text{snap}}^+ \Psi_k = \zeta (R_{\text{snap}}^+)^T M_1^+ R_{\text{snap}}^+ \Psi_k \quad (23)$$

or

$$(R_{\text{snap}}^+)^T A^+ R_{\text{snap}}^+ \Psi_k = \zeta (R_{\text{snap}}^+)^T M_2^+ R_{\text{snap}}^+ \Psi_k \quad (24)$$

in the snapshot space, where

$$\begin{aligned}
A^+ &= [a_{kl}^+] = \int_{K_i^+} \left(2\mu\epsilon(\psi_k^{+, \text{snap}}) : \epsilon(\psi_l^{+, \text{snap}}) + \lambda \nabla \cdot \psi_k^{+, \text{snap}} \nabla \cdot \psi_l^{+, \text{snap}} \right) dx, \\
M_1^+ &= [m_{1,kl}^+] = \frac{1}{H} \int_{K_i^+} \{ \lambda + 2\mu \} \psi_k^{+, \text{snap}} \cdot \psi_l^{+, \text{snap}} dx, \\
M_2^+ &= [m_{2,kl}^+] = \frac{1}{H} \int_{\partial K_i^+} \{ \lambda + 2\mu \} \psi_k^{+, \text{snap}} \cdot \psi_l^{+, \text{snap}} dx.
\end{aligned}$$

After solving above local spectral problems, we form the offline space as in the no oversampling case, see Section 3.1 for CG coupling and Section 3.2 for DG coupling.

4 Numerical result

In this section, we present numerical results for CG-GMsFEM and DG-GMsFEM with two models. We consider different choices of snapshot spaces such as local-fine grid functions and harmonic functions and use different local spectral problems such as no-oversampling and oversampling described in the paper. For the first model, we consider the medium that has no-scale separation and features such as high conductivity channels and isolated inclusions. The Young's modulus $E(x)$ is depicted in Figure 2, $\lambda(x) = \frac{\nu}{(1+\nu)(1-2\nu)}E(x)$, $\mu(x) = \frac{1}{2(1+\nu)}E(x)$, the Poisson ratio ν is taken to be 0.22. For the second example, we use the model that is used in [11] for the simulation of subsurface elastic waves (see Figure 3). In all numerical tests, we use constant force and homogeneous Dirichlet boundary condition. In all tables below, Λ_* represent the minimum discarded eigenvalue of the corresponding spectral problem. We note that the first three eigenbasis are constant and linear functions, therefore we present our numerical results starting from fourth eigenbasis in all cases.

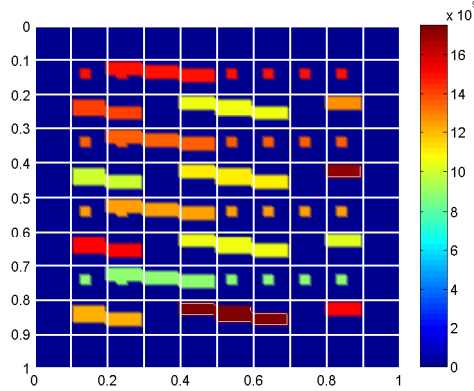


Figure 2: Young's modulus (Model 1)

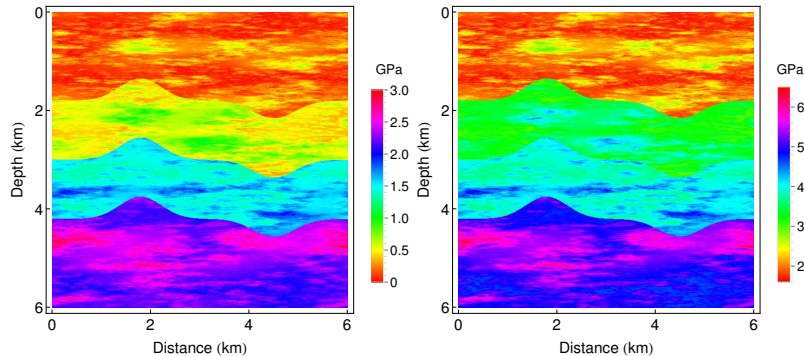


Figure 3: Left: λ Right: μ (Model 2)

Before presenting the numerical results, we summarize our numerical findings.

- We observe a fast decay in the error as more basis functions are added in both CG-GMsFEM and DG-GMsFEM
- We observe the use of multiscale partition of unity improves the accuracy of CG-GMsFEM compared to the use of piecewise bi-linear functions
- We observe an improvement in the accuracy (a slight improvement in CG case and a large improvement in DG case) when using oversampling for the examples we considered and the decrease in the snapshot space dimension

4.1 Numerical results for Model 1 with conforming GMsFEM (CG-GMsFEM)

For the first model, we divide the domain $D = [0, 1] \times [0, 1]$ into 10×10 coarse grid blocks, inside each coarse block we use 10×10 fine scale square blocks, which result in a 100×100 fine grid blocks. The dimension of the reference solution is 20402. We will show the performance of CG-GMsFEM with the use of local fine-scale snapshots and harmonic extension snapshots. Both bi-linear and multiscale partition of unity functions (see section 3.1) will be considered. For each case, we will provide the comparison using oversampling and no-oversampling. For the error measure, we use relative weighted L^2 norm error and weighted H^1 norm error to compare the accuracy of CG-GMsFEM, which is defined as

$$e_{L^2} = \frac{\|(\lambda + 2\mu)(u_H - u_h)\|_{L^2(D)}}{\|(\lambda + 2\mu)u_h\|_{L^2(D)}}, \quad e_{H^1} = \sqrt{\frac{a(u_H - u_h, u_H - u_h)}{a(u_h, u_h)}}$$

where u_H and u_h are CG-GMsFEM defined in (7) and fine-scale CG-FEM solution defined in (4) respectively.

Tables 1 and 2 show the numerical results of using local fine-scale snapshots with piecewise bi-linear function and multiscale functions as partition of unity respectively. As we observe, when using more multiscale basis, the errors decay rapidly, especially for multiscale partition of unity. For example, we can see that the weighted L^2 error drops from 24.9% to 1.1% in the case of using bi-linear function as partition of unity with no oversampling, while the dimension increases from 728 to 2672. If we use multiscale partition of unity, the corresponding weighted L^2 error drops from 8.4% to 0.6%, which demonstrates a great advantage of multiscale partition of unity. Oversampling can help improve the accuracy as our results indicate. The local eigenvalue problem used for oversampling is Eq.(22).

Next, we present the numerical results when harmonic extensions are used as snapshots in Tables 3 and 4. We can observe similar trends as in the local fine-scale snapshot case. The errors decrease as the number of basis functions increase. The L^2 error is less than 1% when about 13% percent of degrees of freedom is used. Similarly, the oversampling method helps to improve the accuracy. In this case, the local eigenvalue problem used for oversampling is Eq.(21).

Dimension	$1/\Lambda_*$		e_{L^2}		e_{H^1}	
	without oversampling	with oversampling	without oversampling	with oversampling	without oversampling	with oversampling
728	1.3e+07	1.4e+07	0.249	0.215	0.444	0.409
1214	3.1e+06	5.6e+06	0.048	0.047	0.220	0.213
1700	7.0e+05	2.7e+06	0.027	0.024	0.162	0.153
2186	1.8e+00	1.7e+06	0.018	0.016	0.133	0.123
2672	9.9e-01	1.4e+06	0.011	0.010	0.105	0.099

Table 1: Relative errors between CG-MsFEM solution and the fine-scale CG-FEM solution, piecewise bi-linear partition of unity functions are used. The case with local fine-scale snapshots.

Dimension	$1/\Lambda_*$		e_{L^2}		e_{H^1}	
	without oversampling	with oversampling	without oversampling	with oversampling	without oversampling	with oversampling
728	6.9e+06	6.2e+06	0.084	0.110	0.254	0.274
1214	5.8e+00	3.2e+06	0.031	0.028	0.166	0.160
1700	2.1e+00	1.2e+06	0.015	0.012	0.111	0.105
2186	1.3e+00	5.9e+05	0.009	0.008	0.088	0.083
2672	9.4e-01	1.0e+01	0.006	0.005	0.071	0.066

Table 2: Relative errors between CG-MsFEM solution and the fine-scale CG-FEM solution, multiscale partition of unity functions are used. The case with local fine-scale snapshots.

Dimension	$1/\Lambda_*$		e_{L^2}		e_{H^1}	
	without oversampling	with oversampling	without oversampling	with oversampling	without oversampling	with oversampling
728	1.3e+07	1.2e+07	0.254	0.218	0.446	0.418
1214	2.1e+06	5.5e+06	0.047	0.048	0.218	0.217
1700	2.8e+05	3.2e+06	0.024	0.022	0.153	0.148
2186	1.2e+00	9.8e+05	0.016	0.015	0.124	0.122
2672	5.8e-01	2.1e+04	0.008	0.010	0.102	0.099

Table 3: Relative errors between CG-MsFEM solution and the fine-scale CG-FEM solution, piecewise bi-linear partition of unity functions are used. The case with hamonic snapshots.

Dimension	$1/\Lambda_*$		e_{L^2}		e_{H^1}	
	without oversampling	with oversampling	without oversampling	with oversampling	without oversampling	with oversampling
728	7.0e+06	7.2e+06	0.087	0.112	0.259	0.291
1214	5.5e+00	3.2e+06	0.034	0.032	0.174	0.169
1700	1.9e+00	1.5e+06	0.015	0.013	0.115	0.112
2186	1.0e+00	2.5e+05	0.009	0.008	0.090	0.089
2672	7.1e-01	1.7e+00	0.007	0.006	0.075	0.074

Table 4: Relative errors between CG-MsFEM solution and the fine-scale CG-FEM solution, multiscale partition of unity functions are used. The case with hamonic snapshots.

Dimension	$1/\Lambda_*$		e_{L^2}		e_{H^1}	
	without oversampling	with oversampling	without oversampling	with oversampling	without oversampling	with oversampling
728	4.9e-03	1.5e-03	0.281	0.141	0.554	0.525
1184	3.0e-03	8.5e-04	0.118	0.019	0.439	0.209
1728	2.1e-03	5.6e-04	0.108	0.012	0.394	0.145
2184	1.2e-03	3.5e-04	0.073	0.007	0.348	0.096
2696	1.0e-03	2.7e-04	0.056	0.002	0.300	0.058

Table 5: Relative errors between DG-MsFEM solution and the fine-scale DG-FEM solution. The case with local fine-scale snapshots.

Dimension	$1/\Lambda_*$		e_{L^2}		e_{H^1}	
	without oversampling	with oversampling	without oversampling	with oversampling	without oversampling	with oversampling
728	2.9e-01	1.6e-01	0.285	0.149	0.557	0.528
1184	1.6e-01	6.5e-02	0.193	0.076	0.515	0.366
1728	1.0e-01	5.4e-02	0.114	0.009	0.432	0.155
2184	7.1e-02	3.9e-02	0.081	0.004	0.326	0.078
2696	6.3e-02	2.8e-02	0.043	0.002	0.231	0.060

Table 6: Relative errors between DG-MsFEM solution and the fine-scale DG-FEM solution. The case with hamonic snapshots.

4.2 Numerical results for Model 1 with DG-GMsFEM

In this section, we consider numerical results for DG-GMsFEM discussed in Section 3.2. To show the performance of DG-GMsFEM, we use the same model (see Figure 2) and the coarse and fine grid settings as in the CG case. We will also present the result of using both harmonic extension and eigenbasis (local fine-scale) as snapshot space. To measure the error, we define broken weighted L^2 norm error and H^1 norm error

$$e_{L^2} = \sqrt{\frac{\sum_{K \in \mathcal{T}_H} \int_K (\lambda + 2\mu)(u_H - u_h)^2 dx}{\sum_{K \in \mathcal{T}_H} \int_K (\lambda + 2\mu)u_h^2 dx}} \quad e_{H^1} = \sqrt{\frac{\sum_{K \in \mathcal{T}_H} \int_K \sigma(u_H - u_h) : \varepsilon(u_H - u_h) dx}{\sum_{K \in \mathcal{T}_H} \int_K \sigma(u_h) : \varepsilon(u_h) dx}}$$

where u_H and u_h are DG-GMsFEM defined in (8) and fine-scale DG-FEM solution defined in (48) respectively.

In Table 5, the numerical results of DG-MsFEM with local fine-scale functions as the snapshot space is shown. We observe that DG-MsFEM shows a better approximation compared to CG-MsFEM if oversampling is used. The error decreases more rapidly as we add basis. More specifically, the relative broken L^2 error and H^1 error decrease from 14.1%, 52.5% to 0.2% and 5.8% respectively, while the degrees of freedom of the coarse system increase from 728 to 2696, where the latter is only 13.2% of the reference solution. The local eigenvalue problem used for oversampling is Eq.(23).

Table 6 shows the corresponding results when harmonic functions are used to construct the snapshot space. We observe similar errors decay trend as local fine-scale snapshots are used. Oversampling can help improve the results significantly. Although the error is very large when the dimension of coarse system is 728 (4 multiscale basis is used), the error becomes very small when the dimension reaches 1728 (9 multiscale basis is used). The local eigenvalue problem used for oversampling here is Eq.(24). We remark that oversampling can not only help decrease the error, but also decrease the dimension of the snapshot space greatly in peridoic case.

4.3 Numerical results for Model 2

The purpose of this example is to test a method for an earth model that is used in [11]. The domain for the second model is $D = (0, 6000)^2$ (in meters) which is divided into $900 = 30 \times 30$ square coarse grid blocks, inside each coarse block we generate 20×20 fine scale square blocks. The reference solution is computed through standard CG-FEM on the resulting 600×600 fine grid. We note that the dimension of the reference solution is 722402. The numerical results for CG-MsFEM and DG-MsFEM are presented in Table 7 and 8 respectively. We observe the relatively low errors compared to the high contrast case and the error decrease with the dimension increase of the offline space. Both coupling methods (CG and DG) show very good approximation ability.

dimension	$\frac{1}{\Lambda_*}$	e_{L^2}	e_{H^1}
6968	4.9e+00	3.1e-03	5.4e-02
8650	4.5e+00	2.7e-03	5.2e-02
10332	3.9e+00	2.5e-03	4.9e-02
12014	3.6e+00	2.2e-03	4.7e-02

Table 7: Relative errors between CG-MsFEM solution and the fine-scale CG-FEM solution, piecewise bi-linear partition of unity functions are used. The case with local fine-scale snapshots.

dimension	$\frac{1}{\Lambda_*}$	e_{L^2}	e_{H^1}
7200	6.3e-06	4.1e-03	7.1e-02
9000	6.0e-06	4.0e-03	6.6e-02
10800	4.6e-06	3.8e-03	6.3e-02
12600	4.5e-06	3.1e-03	5.9e-02

Table 8: Relative errors between DG-MsFEM solution and the fine-scale DG-FEM solution. The case with local fine-scale snapshots.

5 Error estimate for CG coupling

In this section, we present error analysis for both no oversampling and oversampling cases. In the below, $a \preceq b$ means $a \leq Cb$, where C is a constant that is independent of the mesh size and the contrast of the coefficient.

5.1 No oversampling case

Lemma 1 *Let ω_n coarse neighborhood. For any $\psi \in H^1(\omega_n)$, we define $r = -\text{div}(\sigma(\psi))$. Then we have*

$$\int_{\omega_n} 2\mu\chi_n^2 \epsilon(\psi) : \epsilon(\psi) + \int_{\omega_n} \lambda\chi_n^2 (\nabla \cdot \psi)^2 \preceq \left| \int_{\omega_n} \chi_n^2 r \cdot \psi \right| + \int_{\omega_n} (\lambda + 2\mu) |\nabla \chi_n|^2 \psi^2, \quad (25)$$

where χ_n is a scalar partition of unity subordinated to the coarse neighborhood ω_n .

Proof. Multiplying both sides of $-\operatorname{div}(\sigma(\psi)) = r$ by $\chi_n^2\psi$, we have

$$\begin{aligned}
\int_{\omega_n} \chi_n^2 r \cdot \psi &= \int_{\omega_n} 2\mu\epsilon(\psi) : \epsilon(\chi_n^2\psi) + \int_{\omega_n} \lambda \nabla \cdot \psi \nabla \cdot (\chi_n^2\psi) \\
&= \int_{\omega_n} 2\mu\chi_n^2\epsilon(\psi) : \epsilon(\psi) + \int_{\omega_n} 2\mu\chi_n\epsilon_{ij}(\psi)(\psi_i \frac{\partial\chi_n}{\partial x_j} + \psi_j \frac{\partial\chi_n}{\partial x_i}) \\
&\quad + \int_{\omega_n} \lambda\chi_n^2(\nabla \cdot \psi)^2 + \int_{\omega_n} 2\lambda \nabla \cdot \psi \chi_n \psi \cdot \nabla \chi_n \\
&= \int_{\omega_n} 2\mu\chi_n^2\epsilon(\psi) : \epsilon(\psi) + \int_{\omega_n} 2 \left(\sqrt{2\mu}\chi_n\epsilon_{ij}(\psi) \right) \left(\sqrt{\mu/2}(\psi_i \frac{\partial\chi_n}{\partial x_j} + \psi_j \frac{\partial\chi_n}{\partial x_i}) \right) \\
&\quad + \int_{\omega_n} \lambda\chi_n^2(\nabla \cdot \psi)^2 + \int_{\omega_n} 2 \left(\sqrt{\lambda}\chi_n \nabla \cdot \psi \right) \left(\sqrt{\lambda}\psi \cdot \nabla \chi_n \right).
\end{aligned} \tag{26}$$

Therefore,

$$\begin{aligned}
&\int_{\omega_n} 2\mu\chi_n^2\epsilon(\psi) : \epsilon(\psi) + \int_{\omega_n} \lambda\chi_n^2(\nabla \cdot \psi)^2 \\
&\leq \left| \int_{\omega_n} \chi_n^2 r \cdot \psi \right| + \left| \int_{\omega_n} 2 \left(\sqrt{2\mu}\chi_n\epsilon_{ij}(\psi) \right) \left(\sqrt{\mu/2}(\psi_i \frac{\partial\chi_n}{\partial x_j} + \psi_j \frac{\partial\chi_n}{\partial x_i}) \right) + \int_{\omega_n} 2 \left(\sqrt{\lambda}\chi_n \nabla \cdot \psi \right) \left(\sqrt{\lambda}\psi \cdot \nabla \chi_n \right) \right| \\
&\preceq \left| \int_{\omega_n} \chi_n^2 r \cdot \psi \right| + \int_{\omega_n} (2\lambda + 4\mu) |\nabla \chi_n|^2 \psi^2 \\
&\preceq \left| \int_{\omega_n} \chi_n^2 r \cdot \psi \right| + \int_{\omega_n} (\lambda + 2\mu) |\nabla \chi_n|^2 \psi^2.
\end{aligned} \tag{27}$$

In the last step, we have used $2ab \leq \epsilon a^2 + \frac{1}{\epsilon} b^2$, and $(ab + cd)^2 \leq (a^2 + c^2)(b^2 + d^2)$.

□

Next, we will show the convergence of the CG-GMsFEM solution defined in (7) without oversampling. We take $I^{\omega_n}u_h$ to be the first L_n terms of spectral expansion of u in terms of eigenfunctions of the problem $-\operatorname{div}(\sigma(\phi_n)) = \xi \tilde{\kappa} \phi_n$ solved in $V^h(\omega_n)$. Applying Cea's Lemma, Lemma 1 and using the fact that $\chi_n \preceq 1$, we can get

$$\begin{aligned}
&\int_D (2\mu\epsilon(u_h - u_H) : \epsilon(u_h - u_H) + \lambda(\nabla \cdot (u_h - u_H))^2) \\
&\preceq \sum_{n=1}^{N_s} \int_{\omega_n} (2\mu\epsilon(\chi_n(u_h - I^{\omega_n}u_h)) : \epsilon(\chi_n(u_h - I^{\omega_n}u_h)) + \lambda(\nabla \cdot (\chi_n(u_h - I^{\omega_n}u_h)))^2) \\
&\preceq \sum_{n=1}^{N_s} \int_{\omega_n} 2\mu\chi_n^2\epsilon(u_h - I^{\omega_n}u_h) : \epsilon(u_h - I^{\omega_n}u_h) + \sum_{n=1}^{N_s} \int_{\omega_n} \lambda\chi_n^2(\nabla \cdot (u_h - I^{\omega_n}u_h))^2 \\
&\quad + \sum_{n=1}^{N_s} \int_{\omega_n} (\lambda + 2\mu) |\nabla \chi_n|^2 (u_h - I^{\omega_n}u_h)^2 \\
&\preceq \sum_{n=1}^{N_s} \int_{\omega_n} (\lambda + 2\mu) |\nabla \chi_n|^2 (u_h - I^{\omega_n}u_h)^2 + \sum_{n=1}^{N_s} \left| \int_{\omega_n} \chi_n^2 g \cdot (u_h - I^{\omega_n}u_h) \right| \\
&\preceq \sum_{n=1}^{N_s} \int_{\omega_n} (\lambda + 2\mu) |\nabla \chi_n|^2 (u_h - I^{\omega_n}u_h)^2 + \sum_{n=1}^{N_s} \int_{\omega_n} ((\lambda + 2\mu) |\nabla \chi_n|^2)^{-1} g^2,
\end{aligned} \tag{28}$$

where $g = f + \operatorname{div}(\sigma(I^{\omega_n}u_h))$, f is the right hand side of (2).

Using the properties of the eigenfunctions, we obtain

$$\int_{\omega_n} (\lambda + 2\mu) \sum_{s=1}^{N_s} |\nabla \chi_s|^2 (u_h - I^{\omega_n} u_h)^2 \preceq \frac{1}{\xi_{L_n+1}^{\omega_n}} \left(\int_{\omega_n} 2\mu \epsilon(u_h - I^{\omega_n} u_h) : \epsilon(u_h - I^{\omega_n} u_h) + \lambda (\nabla \cdot (u_h - I^{\omega_n} u_h))^2 \right). \quad (29)$$

Then, the first term in the right hand side of (28) can be estimated as follows

$$\begin{aligned} & \sum_{n=1}^{N_s} \int_{\omega_n} (\lambda + 2\mu) |\nabla \chi_n|^2 (u_h - I^{\omega_n} u_h)^2 \preceq \sum_{n=1}^{N_s} \int_{\omega_n} (\lambda + 2\mu) \sum_{s=1}^{N_s} |\nabla \chi_s|^2 (u_h - I^{\omega_n} u_h)^2 \\ & \preceq \sum_{n=1}^{N_s} \frac{1}{\xi_{L_n+1}^{\omega_n}} \left(\int_{\omega_n} 2\mu \epsilon(u_h - I^{\omega_n} u_h) : \epsilon(u_h - I^{\omega_n} u_h) + \int_{\omega_n} \lambda (\nabla \cdot (u_h - I^{\omega_n} u_h))^2 \right) \\ & \preceq \sum_{n=1}^{N_s} \frac{\alpha_{L_n+1}^{\omega_n}}{\xi_{L_n+1}^{\omega_n}} \left(\int_{\omega_n} 2\mu \chi_n^2 \epsilon(u_h - I^{\omega_n} u_h) : \epsilon(u_h - I^{\omega_n} u_h) + \int_{\omega_n} \lambda \chi_n^2 (\nabla \cdot (u_h - I^{\omega_n} u_h))^2 \right) \quad (30) \\ & \preceq \sum_{n=1}^{N_s} \frac{\alpha_{L_n+1}^{\omega_n}}{\xi_{L_n+1}^{\omega_n}} \int_{\omega_n} (\lambda + 2\mu) |\nabla \chi_n|^2 (u_h - I^{\omega_n} u_h)^2 + \sum_{n=1}^{N_s} \frac{\alpha_{L_n+1}^{\omega_n}}{\xi_{L_n+1}^{\omega_n}} \left| \int_{\omega_n} \chi_n^2 g \cdot (u_h - I^{\omega_n} u_h) \right| \\ & \preceq \frac{1}{\Lambda_*} \left(\sum_{n=1}^{N_s} \int_{\omega_n} (\lambda + 2\mu) |\nabla \chi_n|^2 (u_h - I^{\omega_n} u_h)^2 + \sum_{n=1}^{N_s} \left| \int_{\omega_n} \chi_n^2 g \cdot (u_h - I^{\omega_n} u_h) \right| \right), \end{aligned}$$

where

$$\Lambda_* = \min_{\omega_n} \frac{\xi_{L_n+1}^{\omega_n}}{\alpha_{L_n+1}^{\omega_n}},$$

and

$$\alpha_{L_n+1}^{\omega_n} = \frac{\int_{\omega_n} 2\mu \epsilon(u_h - I^{\omega_n} u_h) : \epsilon(u_h - I^{\omega_n} u_h) + \int_{\omega_n} \lambda (\nabla \cdot (u_h - I^{\omega_n} u_h))^2}{\int_{\omega_n} 2\mu \chi_n^2 \epsilon(u_h - I^{\omega_n} u_h) : \epsilon(u_h - I^{\omega_n} u_h) + \int_{\omega_n} \lambda \chi_n^2 (\nabla \cdot (u_h - I^{\omega_n} u_h))^2}.$$

Applying inequality (30) m times, we have

$$\begin{aligned} & \sum_{n=1}^{N_s} \int_{\omega_n} (\lambda + 2\mu) |\nabla \chi_n|^2 (u_h - I^{\omega_n} u_h)^2 \\ & \preceq \left(\frac{1}{\Lambda_*} \right)^m \sum_{n=1}^{N_s} \int_{\omega_n} (\lambda + 2\mu) |\nabla \chi_n|^2 (u_h - I^{\omega_n} u_h)^2 + \sum_{l=1}^m \left(\frac{1}{\Lambda_*} \right)^l \sum_{n=1}^{N_s} \left| \int_{\omega_n} \chi_n^2 g \cdot (u_h - I^{\omega_n} u_h) \right| \\ & \preceq \left(\frac{1}{\Lambda_*} \right)^m \sum_{n=1}^{N_s} \int_{\omega_n} (\lambda + 2\mu) |\nabla \chi_n|^2 (u_h - I^{\omega_n} u_h)^2 + (\Lambda_*)^m \left(\frac{1 - \Lambda_*^{-m}}{\Lambda_* - 1} \right) \sum_{n=1}^{N_s} \int_{\omega_n} ((\lambda + 2\mu) |\nabla \chi_n|^2)^{-1} g^2, \quad (31) \end{aligned}$$

Taking into account that

$$\sum_{n=1}^{N_s} \int_{\omega_n} (\lambda + 2\mu) |\nabla \chi_n|^2 (u_h - I^{\omega_n} u_h)^2 \preceq \sum_{n=1}^{N_s} \int_{\omega_n} (\lambda + 2\mu) \sum_{s=1}^{N_s} |\nabla \chi_s|^2 (u_h - I^{\omega_n} u_h)^2, \quad (32)$$

and

$$\sum_{n=1}^{N_s} \int_{\omega_n} (2\mu \epsilon(u_h - I^{\omega_n} u_h) : \epsilon(u_h - I^{\omega_n} u_h) + \lambda (\nabla \cdot (u_h - I^{\omega_n} u_h))^2) \preceq \int_D (2\mu \epsilon(u_h) : \epsilon(u) + \lambda (\nabla \cdot u_h)^2). \quad (33)$$

inequality (28) becomes

$$\begin{aligned}
& \int_D (2\mu\epsilon(u_h - u_H) : \epsilon(u_h - u_H) + \lambda(\nabla \cdot (u_h - u_H))^2) \\
& \preceq \left(\frac{1}{\Lambda_*}\right)^{m+1} \left(\sum_{n=1}^{N_s} \int_{\omega_n} 2\mu\epsilon(u_h - I^{\omega_n} u_h) : \epsilon(u_h - I^{\omega_n} u_h) + \sum_{n=1}^{N_s} \int_{\omega_n} \lambda(\nabla \cdot (u_h - I^{\omega_n} u_h))^2 \right) \\
& \quad + \left(\Lambda_*^m \left(\frac{1 - \Lambda_*^{-m}}{\Lambda_* - 1} \right) + 1 \right) \sum_{n=1}^{N_s} \int_{\omega_n} ((\lambda + 2\mu)|\nabla\chi_n|^2)^{-1} g^2 \\
& \preceq \left(\frac{1}{\Lambda_*}\right)^{m+1} \int_D (2\mu\epsilon(u_h) : \epsilon(u) + \lambda(\nabla \cdot u_h)^2) + \left((\Lambda_*)^m \left(\frac{1 - (\Lambda_*)^{-m}}{\Lambda_* - 1} \right) + 1 \right) R,
\end{aligned} \tag{34}$$

where $R = \sum_{n=1}^{N_s} \int_{\omega_n} ((\lambda + 2\mu)|\nabla\chi_n|^2)^{-1} g^2$. If $|g| \preceq 1$, then $\int_{\omega_n} ((\lambda + 2\mu)|\nabla\chi_n|^2)^{-1} g^2 \preceq H^2$, from which we obtain

$$\begin{aligned}
\int_D (2\mu\epsilon(u_h - u_H) : \epsilon(u_h - u_H) + \lambda(\nabla \cdot (u_h - u_H))^2) & \preceq \left(\frac{1}{\Lambda_*}\right)^{m+1} \int_D (2\mu\epsilon(u_h) : \epsilon(u) + \lambda(\nabla \cdot u_h)^2) \\
& \quad + \left((\Lambda_*)^m \left(\frac{1 - (\Lambda_*)^{-m}}{\Lambda_* - 1} \right) + 1 \right) H^2.
\end{aligned} \tag{35}$$

Combining results above, we have

Theorem 1 *Let $u \in V_{CG}^h$ be the fine-scale CG-FEM solution defined in (4) and u_H be the CG-GMsFEM solution defined in (7) without oversampling. If $\Lambda_* \geq 1$ and $\int_D (\lambda + 2\mu)^{-1} g^2 \preceq 1$, let $n = -\frac{\log(H)}{\log\Lambda_*}$, then*

$$\int_D (2\mu\epsilon(u_h - u_H) : \epsilon(u_h - u_H) + \lambda(\nabla \cdot (u_h - u_H))^2) \preceq \left(\frac{H}{\Lambda_*}\right) \left(\int_D (2\mu\epsilon(u) : \epsilon(u) + \lambda(\nabla \cdot u_h)^2) + 1 \right).$$

5.2 Oversampling case

In this subsection, we will analyze the convergence of CG-GMsFEM solution defined in (7) with oversampling. We define $I^{\omega_n^+} u_h$ as an interpolation of u_h in ω_n^+ using the first L_n modes for the eigenvalue problem (21). Let χ_n^+ be a partition of unity subordinated to the coarse neighborhood ω_n^+ . We require χ_n^+ to be zero on $\partial\omega_n^+$ and

$$|\nabla\chi_n|^2 \preceq |\nabla\chi_n^+|^2.$$

Using the same argument as Lemma 1, it is easy to deduce

$$\begin{aligned}
& \int_{\omega_n^+} \left(2\mu|\chi_n^+|^2 \epsilon(u_h - I^{\omega_n^+} u_h) : \epsilon(u_h - I^{\omega_n^+} u_h) + \lambda|\chi_n^+|^2 (\nabla \cdot (u_h - I^{\omega_n^+} u_h))^2 \right) \\
& \preceq \int_{\omega_n^+} |\chi_n^+|^2 g \cdot (u_h - I^{\omega_n^+} u_h) + \int_{\omega_n^+} (\lambda + 2\mu) |\nabla\chi_n^+|^2 (u_h - I^{\omega_n^+} u_h)^2,
\end{aligned} \tag{36}$$

where $g = f + \text{div}(\sigma(I^{\omega_n} u_h))$, $I^{\omega_n} u_h = I^{\omega_n^+} u_h$ in ω_n .

Applying eigenvalue problem (21), we obtain

$$\int_{\omega_n^+} (\lambda + 2\mu) |\nabla\chi_n^+|^2 (u_h - I^{\omega_n^+} u_h)^2 \preceq \frac{1}{\xi_{L_n+1}^{\omega_n}} \int_{\omega_n} (2\mu\epsilon(u_h - I^{\omega_n} u_h) : \epsilon(u_h - I^{\omega_n} u_h) + \lambda(\nabla \cdot (u_h - I^{\omega_n} u_h))^2). \tag{37}$$

Using the definition of interpolation $I^{\omega_n^+} u_h$, we have

$$\begin{aligned}
& \sum_{n=1}^{N_s} \int_{\omega_n} (\lambda + 2\mu) |\nabla \chi_n|^2 (u_h - I^{\omega_n} u_h)^2 \preceq \sum_{n=1}^{N_s} \int_{\omega_n^+} (\lambda + 2\mu) |\nabla \chi_n^+|^2 (u_h - I^{\omega_n^+} u_h)^2 \\
& \preceq \sum_{n=1}^{N_s} \frac{1}{\xi_{L_{n+1}}^{\omega_n}} \left(\int_{\omega_n} 2\mu \epsilon(u_h - I^{\omega_n} u_h) : \epsilon(u_h - I^{\omega_n} u_h) + \int_{\omega_n} \lambda (\nabla \cdot (u_h - I^{\omega_n} u_h))^2 \right) \\
& \preceq \sum_{n=1}^{N_s} \frac{1}{\xi_{L_{n+1}}^{\omega_n}} \left(\int_{\omega_n^+} 2\mu |\nabla \chi_n^+|^2 \epsilon(u_h - I^{\omega_n^+} u_h) : \epsilon(u_h - I^{\omega_n^+} u_h) + \int_{\omega_n^+} \lambda |\nabla \chi_n^+|^2 (\nabla \cdot (u_h - I^{\omega_n^+} u_h))^2 \right) \\
& \preceq \sum_{n=1}^{N_s} \frac{1}{\xi_{L_{n+1}}^{\omega_n}} \int_{\omega_n^+} (\lambda + 2\mu) |\nabla \chi_n^+|^2 (u_h - I^{\omega_n^+} u_h)^2 + \sum_{n=1}^{N_s} \frac{1}{\xi_{L_{n+1}}^{\omega_n}} \left| \int_{\omega_n^+} |\chi_n^+|^2 g \cdot (u_h - I^{\omega_n^+} u_h) \right| \\
& \preceq \frac{1}{\Lambda_*^+} \left(\sum_{n=1}^{N_s} \int_{\omega_n^+} (\lambda + 2\mu) |\nabla \chi_n^+|^2 (u_h - I^{\omega_n^+} u_h)^2 + \sum_{n=1}^{N_s} \left| \int_{\omega_n^+} |\chi_n^+|^2 g \cdot (u_h - I^{\omega_n^+} u_h) \right| \right) \\
& \preceq \frac{1}{\Lambda_*^+} \sum_{n=1}^{N_s} \left(\frac{1}{\xi_{L_{n+1}}^{\omega_n}} \int_{\omega_n} (2\mu \epsilon(u_h - I^{\omega_n} u_h) : \epsilon(u_h - I^{\omega_n} u_h) + \lambda (\nabla \cdot (u_h - I^{\omega_n} u_h))^2) + \left| \int_{\omega_n^+} |\chi_n^+|^2 g \cdot (u_h - I^{\omega_n^+} u) \right| \right), \tag{38}
\end{aligned}$$

where $\Lambda_*^+ = \min_{\omega_n} \xi_{L_{n+1}}^{\omega_n}$.

Applying the last inequality m times with (37), we get

$$\begin{aligned}
& \int_{\omega_n^+} (\lambda + 2\mu) |\nabla \chi_n^+|^2 (u_h - I^{\omega_n^+} u_h)^2 \\
& \preceq \left(\frac{1}{\Lambda_*^+} \right)^m \left(\frac{1}{\xi_{L_{n+1}}^{\omega_n}} \int_{\omega_n} 2\mu \epsilon(u_h - I^{\omega_n} u_h) : \epsilon(u_h - I^{\omega_n} u_h) + \frac{1}{\xi_{L_{n+1}}^{\omega_n}} \int_{\omega_n} \lambda (\nabla \cdot (u_h - I^{\omega_n} u_h))^2 \right) \\
& \quad + \sum_{l=1}^m \left(\frac{1}{\Lambda_*^+} \right)^l \sum_{n=1}^{N_s} \left| \int_{\omega_n^+} |\chi_n^+|^2 g \cdot (u_h - I^{\omega_n^+} u_h) \right| \\
& \preceq \left(\frac{1}{\Lambda_*^+} \right)^{m+1} \left(\int_{\omega_n} 2\mu \epsilon(u_h - I^{\omega_n} u_h) : \epsilon(u_h - I^{\omega_n} u_h) + \int_{\omega_n} \lambda (\nabla \cdot (u_h - I^{\omega_n} u_h))^2 \right) \\
& \quad + (\Lambda_*^+)^m \left(\frac{1 - (\Lambda_*^+)^{-m}}{\Lambda_*^+ - 1} \right) \sum_{n=1}^{N_s} \int_{\omega_n^+} ((\lambda + 2\mu) |\nabla \chi_n|^2)^{-1} g^2. \tag{39}
\end{aligned}$$

Taking into account inequality (33), we have

$$\begin{aligned}
& \int_D (2\mu \epsilon(u_h - u_H) : \epsilon(u_h - u_H) + \lambda (\nabla \cdot (u_h - u_H))^2) \\
& \preceq \sum_{n=1}^{N_s} \int_{\omega_n} (\lambda + 2\mu) |\nabla \chi_n|^2 (u_h - I^{\omega_n} u_h)^2 + \sum_{n=1}^{N_s} \left| \int_{\omega_n} \chi_n^2 g \cdot (u_h - I^{\omega_n} u_h) \right| \\
& \preceq \left(\frac{1}{\Lambda_*^+} \right)^{m+1} \int_D (2\mu \epsilon(u) : \epsilon(u) + \lambda (\nabla \cdot u_h)^2) + \left((\Lambda_*^+)^m \left(\frac{1 - (\Lambda_*^+)^{-m}}{\Lambda_*^+ - 1} \right) + 1 \right) R. \tag{40}
\end{aligned}$$

where $R = \sum_{n=1}^{N_s} \int_{\omega_n} ((\lambda + 2\mu) |\nabla \chi_n^+|^2)^{-1} g^2$.

Therefore, similar with the no oversampling case, we have

Theorem 2 *Let $u \in V_{CG}^h$ be the fine-scale CG-FEM solution defined in (4) and u_H be the CG-GMsFEM solution defined in (7) with oversampling. If $\Lambda_*^+ \geq 1$ and $\int_D (\lambda + 2\mu)^{-1} g^2 \preceq 1$, let $n = -\frac{\log(H)}{\log \Lambda_*^+}$, then*

$$\int_D (2\mu \epsilon(u_h - u_H) : \epsilon(u_h - u_H) + \lambda (\nabla \cdot (u_h - u_H))^2) \preceq \frac{H}{\Lambda_*^+} \left(\int_D (2\mu \epsilon(u) : \epsilon(u) + \lambda (\nabla \cdot u_h)^2) + 1 \right).$$

6 Error estimate for DG coupling

In this section, we will analyze the DG coupling of the GMsFEM (8). For any u , we define the DG-norm by

$$\|u\|_{\text{DG}}^2 = a_H(u, u) + \sum_{E \in \mathcal{E}^H} \frac{\gamma}{h} \int_E \{\lambda + 2\mu\} [u]^2 ds.$$

Let K be a coarse grid block and let $n_{\partial K}$ be the unit outward normal vector on ∂K . We denote $V^h(\partial K)$ by the restriction of the conforming space V^h on ∂K . The normal flux $\sigma(u) n_{\partial K}$ is understood as an element in $V^h(\partial K)$ and is defined by

$$\int_{\partial K} (\sigma(u) n_{\partial K}) \cdot v = \int_K \left(2\mu \epsilon(u) : \epsilon(\hat{v}) + \lambda \nabla \cdot u \nabla \cdot \hat{v} \right) dx, \quad v \in V^h(\partial K), \quad (41)$$

where \hat{v} is the harmonic extension of v in K . By the Cauchy-Schwarz inequality,

$$\int_{\partial K} (\sigma(u) n_{\partial K}) \cdot v \leq a_H^K(u, u)^{\frac{1}{2}} a_H^K(\hat{v}, \hat{v})^{\frac{1}{2}}.$$

By an inverse inequality and the fact that \hat{v} is the harmonic extension of v

$$a_H^K(\hat{v}, \hat{v}) \leq \kappa_K C_{\text{inv}}^2 h^{-1} \int_{\partial K} |v|^2 dx,$$

where $\kappa_K = \max_K \{\lambda + 2\mu\}$ and $C_{\text{inv}} > 0$ is the constant from inverse inequality. Thus,

$$\int_{\partial K} (\sigma(u) n_{\partial K}) \cdot v \leq \kappa_K^{\frac{1}{2}} C_{\text{inv}} h^{-\frac{1}{2}} \|v\|_{L^2(\partial K)} a_H^K(u, u)^{\frac{1}{2}}.$$

This shows that

$$\int_{\partial K} |\sigma(u) n_{\partial K}|^2 \leq \kappa_K C_{\text{inv}}^2 h^{-1} a_H^K(u, u).$$

Our first step in the convergence analysis is to establish the continuity and the coercivity of the bilinear form (9) with respect to the DG-norm.

Lemma 2 *Assume that the penalty parameter γ is chosen so that $\gamma > 2C_{\text{inv}}^2$. The bilinear form a_{DG} defined in (9) is continuous and coercive, that is,*

$$a_{\text{DG}}(u, v) \leq \|u\|_{\text{DG}} \|v\|_{\text{DG}}, \quad (42)$$

$$a_{\text{DG}}(u, u) \geq a_0 \|u\|_{\text{DG}}^2, \quad (43)$$

for all u, v , where $a_0 = 1 - \sqrt{2}C_{\text{inv}}\gamma^{-\frac{1}{2}} > 0$.

Proof. By the definition of a_{DG} , we have

$$a_{\text{DG}}(u, v) = a_H(u, v) - \sum_{E \in \mathcal{E}^H} \int_E \left(\{\sigma(u) n_E\} \cdot [v] + \{\sigma(v) n_E\} \cdot [u] \right) ds + \sum_{E \in \mathcal{E}^H} \frac{\gamma}{h} \int_E \{\lambda + 2\mu\} [u] \cdot [v] ds.$$

Notice that

$$a_H(u, v) + \sum_{E \in \mathcal{E}^H} \frac{\gamma}{h} \int_E \{\lambda + 2\mu\} [u] \cdot [v] ds \leq \|u\|_{\text{DG}} \|v\|_{\text{DG}}.$$

For an interior coarse edge $E \in \mathcal{E}^H$, we let $K^+, K^- \in \mathcal{T}^H$ be the two coarse grid blocks having the edge E . By the Cauchy-Schwarz inequality, we have

$$\int_E \{\sigma(u) n_E\} \cdot [v] ds \leq \left(h \int_E \{\sigma(u) n_E\}^2 \{\lambda + 2\mu\}^{-1} ds \right)^{\frac{1}{2}} \left(\frac{1}{h} \int_E \{\lambda + 2\mu\} [v]^2 ds \right)^{\frac{1}{2}}. \quad (44)$$

Notice that

$$\begin{aligned} & h \int_E \{\sigma(u) n_E\}^2 \{\lambda + 2\mu\}^{-1} ds \\ & \leq h \left(\int_E (\sigma(u^+) n_E)^2 (\lambda^+ + 2\mu^+)^{-1} ds + \int_E (\sigma(u^-) n_E)^2 (\lambda^- + 2\mu^-)^{-1} ds \right), \end{aligned}$$

where $u^\pm = u|_{K^\pm}$, $\lambda^\pm = \lambda|_{K^\pm}$ and $\mu^\pm = \mu|_{K^\pm}$. So, we have

$$h \int_E \{\sigma(u) n_E\}^2 \{\lambda + 2\mu\}^{-1} ds \leq C_{\text{inv}}^2 \left(a_H^{K^+}(u^+, u^+) + a_H^{K^-}(u^-, u^-) \right).$$

Thus (44) becomes

$$\int_E \{\sigma(u) n_E\} \cdot \llbracket v \rrbracket ds \leq C_{\text{inv}} \left(a_H^{K^+}(u^+, u^+) + a_H^{K^-}(u^-, u^-) \right)^{\frac{1}{2}} \left(\frac{1}{h} \int_E \{\lambda + 2\mu\} \llbracket v \rrbracket^2 ds \right)^{\frac{1}{2}}. \quad (45)$$

When E is a boundary edge, we have

$$\int_E \{\sigma(u) n_E\} \cdot \llbracket v \rrbracket ds \leq C_{\text{inv}} a_H^K(u, u)^{\frac{1}{2}} \left(\frac{1}{h} \int_E \{\lambda + 2\mu\} \llbracket v \rrbracket^2 ds \right)^{\frac{1}{2}}, \quad (46)$$

where K denotes the coarse grid block having the edge E . Summing (45) and (46) for all edges $E \in \mathcal{E}^H$, we have

$$\sum_{E \in \mathcal{E}^H} \int_E \{\sigma(u) n_E\} \cdot \llbracket v \rrbracket ds \leq \sqrt{2} C_{\text{inv}} a_H(u, u)^{\frac{1}{2}} \left(\sum_{E \in \mathcal{E}^H} \frac{1}{h} \int_E \{\lambda + 2\mu\} \llbracket v \rrbracket^2 ds \right)^{\frac{1}{2}}.$$

Similarly, we have

$$\sum_{E \in \mathcal{E}^H} \int_E \{\sigma(v) n_E\} \cdot \llbracket u \rrbracket ds \leq \sqrt{2} C_{\text{inv}} a_H(v, v)^{\frac{1}{2}} \left(\sum_{E \in \mathcal{E}^H} \frac{1}{h} \int_E \{\lambda + 2\mu\} \llbracket u \rrbracket^2 ds \right)^{\frac{1}{2}}.$$

Hence

$$\sum_{E \in \mathcal{E}^H} \int_E \left(\{\sigma(u) n_E\} \cdot \llbracket v \rrbracket + \{\sigma(v) n_E\} \cdot \llbracket u \rrbracket \right) ds \leq \sqrt{2} C_{\text{inv}} \gamma^{-\frac{1}{2}} \|u\|_{\text{DG}} \|v\|_{\text{DG}}. \quad (47)$$

This proves the continuity.

For coercivity, we have

$$a_{\text{DG}}(u, u) = \|u\|_{\text{DG}}^2 - \sum_{E \in \mathcal{E}^H} \int_E \left(\{\sigma(u) n_E\} \cdot \llbracket u \rrbracket + \{\sigma(u) n_E\} \cdot \llbracket u \rrbracket \right) ds.$$

By (47), we have

$$a_{\text{DG}}(u, u) \geq (1 - \sqrt{2} C_{\text{inv}} \gamma^{-\frac{1}{2}}) \|u\|_{\text{DG}}^2,$$

which gives the desired result. \square

We will now prove the convergence of the method (8). Let $u_h \in V_{\text{DG}}^h$ be the fine grid solution which satisfies

$$a_{\text{DG}}(u_h, v) = (f, v), \quad \forall v \in V_{\text{DG}}^h. \quad (48)$$

It is well-known that u_h converges to the exact solution u in the DG-norm as the fine mesh size $h \rightarrow 0$. Next, we define a projection $u_S \in V^{\text{snap}}$ of u_h in the snapshot space by the following construction. For each coarse grid block K , the restriction of u_S on K is defined as the harmonic extension of u_h , that is,

$$\begin{aligned} -\nabla \cdot \sigma(u_S) &= 0, & \text{in } K, \\ u_S &= u_h, & \text{on } \partial K. \end{aligned} \quad (49)$$

Now, we prove the following estimate for the projection u_S .

Lemma 3 Let $u_h \in V_{DG}^h$ be the fine grid solution defined in (48) and $u_S \in V^{snap}$ be the projection of u_h defined in (49). Then we have

$$\|u_h - u_S\|_{DG} \leq CH \left(\max_{K \in \mathcal{T}^H} \eta_K \right) \|f\|_{L^2(\Omega)},$$

where $\eta_K = \min_K \{\lambda + 2\mu\}$.

Proof. Let K be a given coarse grid block. Since $u_S = u_h$ on ∂K , the jump terms in the DG-norm vanish. Thus, the DG-norm can be written as

$$\|u_h - u_S\|_{DG}^2 = \sum_{K \in \mathcal{T}^H} a_H^K(u_h - u_S, u_h - u_S).$$

Since u_S satisfies (49) and $u_h - u_S = 0$ on ∂K , we have

$$a_H^K(u_S, u_h - u_S) = 0.$$

So,

$$\|u_h - u_S\|_{DG}^2 = \sum_{K \in \mathcal{T}^H} a_H^K(u_h, u_h - u_S) = a_{DG}(u_h, u_h - u_S) = (f, u_h - u_S).$$

By the Poincare inequality, we have

$$\|u_h - u_S\|_{L^2(K)} \leq CH^2 \eta_K^2 a_H^K(u_h - u_S, u_h - u_S),$$

where $\eta_K = \min_K \{\lambda + 2\mu\}$. Hence, we have

$$\|u_h - u_S\|_{DG} \leq CH \left(\max_{K \in \mathcal{T}^H} \eta_K \right) \|f\|_{L^2(\Omega)}.$$

□

In the following theorem, we will state and prove the convergence of the GMsFEM (8).

Theorem 3 Let $u_h \in V_{DG}^h$ be the fine grid solution defined in (48) and u_H be the GMsFEM solution defined in (8). Then we have

$$\|u_h - u_H\|_{DG}^2 \leq C \left(\sum_{i=1}^{N_E} \frac{H}{\langle \lambda + 2\mu \rangle \xi_{L_{i+1}}} \left(1 + \frac{\gamma H}{h \xi_{L_{i+1}}}\right) \int_{\partial K_i} (\sigma(u_S) \cdot n_{\partial K})^2 ds + H^2 \left(\max_{K \in \mathcal{T}^H} \eta_K^2 \right) \|f\|_{L^2(\Omega)}^2 \right),$$

where u_S is defined in (49).

Proof. First, we will define a projection $\widehat{u}_S \in V^{\text{off}}$ of u_S in the offline space. Notice that, on each K_i , u_S can be represented by

$$u_S = \sum_{l=1}^{M_i} c_l \psi_l^{i, \text{off}},$$

where $M_i = M^{i, \text{snap}}$ and we assume that the functions $\psi_l^{i, \text{off}}$ are normalized so that

$$\int_{\partial K_i} (\lambda + 2\mu) (\psi_l^{i, \text{off}})^2 ds = 1.$$

Then the function \widehat{u}_S is defined by

$$\widehat{u}_S = \sum_{l=1}^{L_i} c_l \psi_l^{i, \text{off}}.$$

We will find an estimate of $\|u_S - \hat{u}_S\|_{\text{DG}}$. Let K be a given coarse grid block. Recall that the spectral problem is

$$\int_K 2\mu\epsilon(u) : \epsilon(v) dx + \int_K \lambda \nabla \cdot u \nabla \cdot v = \frac{\xi}{H} \int_{\partial K} \langle \lambda + 2\mu \rangle uv ds.$$

By the definition of the flux (41), the spectral problem can be represented as

$$\int_{\partial K} (\sigma(u) \cdot n_{\partial K}) v ds = \frac{\xi}{H} \int_{\partial K} \langle \lambda + 2\mu \rangle uv ds.$$

By the definition of the DG-norm, the error $\|u_S - \hat{u}_S\|_{\text{DG}}$ can be computed as

$$\|\hat{u}_S - u_S\|_{\text{DG}}^2 \leq \sum_K \left(\int_K 2\mu\epsilon(\hat{u}_S - u_S)^2 + \int_K \lambda (\nabla \cdot (\hat{u}_S - u_S))^2 + \frac{\gamma}{h} \int_{\partial K} \{\lambda + 2\mu\} (\hat{u}_S - u_S)^2 \right).$$

Note that

$$\int_{K_i} 2\mu\epsilon(\hat{u}_S - u_S)^2 + \int_{K_i} \lambda (\nabla \cdot (\hat{u}_S - u_S))^2 \leq \frac{1}{h} \int_{\partial K_i} \langle \lambda + 2\mu \rangle (\hat{u}_S - u_S)^2 = \sum_{l=L_i+1}^{M_i} \frac{\xi_l}{H} c_l^2 \leq \frac{H}{\xi_{L_i+1}} \sum_{l=L_i+1}^{M_i} \left(\frac{\xi_l}{H}\right)^2 c_l^2.$$

Also,

$$\frac{1}{h} \int_{\partial K_i} \{\lambda + 2\mu\} (\hat{u}_S - u_S)^2 = \frac{1}{h} \sum_{l=L_i+1}^{M_i} c_l^2 \leq \frac{H^2}{h \xi_{L_i+1}^2} \sum_{l=L_i+1}^{M_i} \left(\frac{\xi_l}{H}\right)^2 c_l^2.$$

Moreover,

$$\sum_{l=L_i+1}^{M_i} \left(\frac{\xi_l}{H}\right)^2 c_l^2 \leq \sum_{l=1}^{M_i} \left(\frac{\xi_l}{H}\right)^2 c_l^2 \leq \frac{1}{\langle \lambda + 2\mu \rangle} \int_{\partial K_i} (\sigma(u_S) \cdot n_{\partial K})^2 ds.$$

Consequently, we obtain the following bound

$$\|u_S - \hat{u}_S\|_{\text{DG}}^2 \leq \sum_{i=1}^{N_E} \frac{H}{\langle \lambda + 2\mu \rangle \xi_{L_i+1}} \left(1 + \frac{\gamma H}{h \xi_{L_i+1}}\right) \int_{\partial K_i} (\sigma(u_S) \cdot n_{\partial K})^2 ds.$$

Next, we will prove the required error bound. By coercivity,

$$\begin{aligned} a_0 \|\hat{u}_S - u_H\|_{\text{DG}}^2 &= a_{\text{DG}}(\hat{u}_S - u_H, \hat{u}_S - u_H) \\ &= a_{\text{DG}}(\hat{u}_S - u_H, \hat{u}_S - u_S) + a_{\text{DG}}(\hat{u}_S - u_H, u_S - u_h) + a_{\text{DG}}(\hat{u}_S - u_H, u_h - u_H). \end{aligned}$$

Note that $a_{\text{DG}}(\hat{u}_S - u_H, u_h - u_H) = 0$ since $\hat{u} - u_H \in V^{\text{off}}$. Using the above results,

$$\|\hat{u}_S - u_H\|_{\text{DG}}^2 \leq C \left(\sum_{i=1}^{N_E} \frac{H}{\langle \lambda + 2\mu \rangle \xi_{L_i+1}} \left(1 + \frac{\gamma H}{h \xi_{L_i+1}}\right) \int_{\partial K_i} (\sigma(u_S) \cdot n_{\partial K})^2 ds + H^2 \left(\max_{K \in \mathcal{T}^H} \eta_K^2 \right) \|f\|_{L^2(\Omega)}^2 \right).$$

Finally, the desired bound is obtained by the triangle inequality

$$\|u_h - u_H\|_{\text{DG}} \leq \|u_h - u_S\|_{\text{DG}} + \|u_S - \hat{u}_S\|_{\text{DG}} + \|\hat{u}_S - u_H\|_{\text{DG}}.$$

□

7 Conclusions

In this paper, we design a multiscale model reduction method using GMsFEM for elasticity equations in heterogeneous media. We design a snapshot space and an offline space based on the analysis. We present two approaches that couple multiscale basis functions of the offline space. These are continuous Galerkin and discontinuous Galerkin methods. Both approaches are analyzed. We present oversampling studies where larger domains are used for calculating the snapshot space. Numerical results are presented.

References

- [1] Assyr Abdulle. Analysis of a heterogeneous multiscale fem for problems in elasticity. *Mathematical Models and Methods in Applied Sciences*, 16(04):615–635, 2006.
- [2] Marco Buck, Oleg Iliev, and Heiko Andrä. Multiscale finite element coarse spaces for the application to linear elasticity. *Central European Journal of Mathematics*, 11(4):680–701, 2013.
- [3] Li-Qun Cao. Iterated two-scale asymptotic method and numerical algorithm for the elastic structures of composite materials. *Computer methods in applied mechanics and engineering*, 194(27):2899–2926, 2005.
- [4] E. Chung, Y. Efendiev, and C. S. Lee. Generalized mixed multiscale finite element method for flows in heterogeneous media. 2014. submitted.
- [5] Y. Efendiev, J. Galvis, and T. Hou. Generalized multiscale finite element methods. *JCP*, 251:116–135, 2013.
- [6] Y. Efendiev, J. Galvis, R. Lazarov, M. Moon, and M. Sarkis. Generalized multiscale finite element method. symmetric interior penalty coupling. *Journal of Computational Physics*, 255(0):1 – 15, 2013.
- [7] Y. Efendiev, J. Galvis, G. Li, and M. Presho. Generalized multiscale finite element methods. over-sampling strategies. *IJMM*.
- [8] Y. Efendiev, R. Lazarov, M. Moon, and K. Shi. A spectral multiscale hybridizable discontinuous galerkin method for second order elliptic problems. *CMAME*, 2014. submitted.
- [9] Y. Efendiev, R. Lazarov, and K. Shi. A multiscale HDG method for second order elliptic equations. Part I. Polynomial and homogenization-based multiscale spaces. *ArXiv e-prints*, October 2013.
- [10] Gilles A Francfort and François Murat. Homogenization and optimal bounds in linear elasticity. *Archive for Rational Mechanics and Analysis*, 94(4):307–334, 1986.
- [11] K. Gao, S. Fu, R. Gibson, E. Chung, and Y. Efendiev. Generalized multiscale finite element method for elastic wave equations. *Expanded SEG Abstracts 2014*. submitted.
- [12] Xiao-Qi Liu, Li-Qun Cao, and Qi-Ding Zhu. Multiscale algorithm with high accuracy for the elastic equations in three-dimensional honeycomb structures. *Journal of computational and applied mathematics*, 233(4):905–921, 2009.
- [13] Olga Arsen’evna Oleinik, AS Shamaev, and GA Yosifian. *Mathematical problems in elasticity and homogenization*, volume 2. Elsevier, 2009.
- [14] Jörg Schröder. A numerical two-scale homogenization scheme: the fe2-method. In *Plasticity and Beyond*, pages 1–64. Springer, 2014.
- [15] Pham Chi Vinh and Do Xuan Tung. Homogenized equations of the linear elasticity theory in two-dimensional domains with interfaces highly oscillating between two circles. *Acta mechanica*, 218(3-4):333–348, 2011.